Role of Normal Stress in the Creep Dynamics and Failure of a Biopolymer Gel

Angelo Pommella,[†] Luca Cipelletti,[*,‡] and Laurence Ramos
Laboratoire Charles Coulomb (L2C), Université Montpellier, CNRS, Montpellier, France

(Received 5 April 2020; revised 6 November 2020; accepted 8 December 2020; published 31 December 2020)

We investigate the delayed rupture of biopolymer gels under a constant shear load by simultaneous dynamic light scattering and rheology measurements. We unveil the crucial role of normal stresses built up during gelation: All samples that eventually fracture self-weaken during the gelation process, as revealed by a partial relaxation of the normal stress concomitant to a burst of microscopic plastic rearrangements. Upon applying a shear stress, weakened gels exhibit in the creep regime distinctive signatures in their microscopic dynamics, which anticipate macroscopic fracture by up to thousands of seconds. The dynamics in fracturing gels are faster than those of nonfracturing gels and exhibit large spatiotemporal fluctuations. A spatially localized region with significant plasticity eventually nucleates, expands progressively, and finally invades the whole sample, triggering macroscopic failure.

DOI: 10.1103/PhysRevLett.125.268006

Failure in soft materials is important from scientific and practical perspectives [1]. Understanding how and when failure may occur is crucial to design materials that are able to prevent or, conversely, to facilitate rupture, depending on applications. Furthermore, why failure may occur after a long induction time is a fascinating question, crucial in fields such as geology, economics, and medicine [2]. In soft matter, many key questions remain unanswered in spite of recent progress in understanding failure phenomena in polymers [3], granular materials [4,5] and networks formed by colloids [6,7], and biopolymers [8–16].

Biopolymer gels are very relevant and largely exploited in drug delivery, personal care, and tissue engineering, thanks to remarkable properties such as high water content and softness. Another distinctive feature of biopolymers forming fibrils is their ability to develop a negative normal stress under shear, due to the stiffness of the fibrils [17–21]. This property is responsible for strain hardening, which allows the gels to stiffen under a large load to prevent rupture, while preserving flexibility at smaller loads. Despite the relevance of these materials, little is known on the microscopic mechanisms leading to failure and their interplay with the distinctive mechanical features of biopolymer gels. Indeed, most studies have focused on crack nucleation and propagation at the macroscopic level [8,10,22] rather than on the evolution of the microscopic structure and dynamics before failure.

We address these questions by coupling dynamic light scattering to rheology to rationalize the failure process of biopolymer gels. We demonstrate the crucial role of normal stresses developed during gelation for the ultimate behavior of the gel under a constant shear load, showing that gels that eventually fail have suffered irreversible damages due to tensile stress self-generated during gelation. We propose that these irreversible rearrangements modify the bond distribution in the sample, ultimately diminishing its resistance to shear stress. Finally, we unveil several kinds of dynamic precursors of failure, highlighting the crucial role of microscopic dynamics for understanding failure in soft materials.

We perform creep tests on agarose gels [23–25], using a rheometer coupled to a custom-made light scattering apparatus [26]. Gelation is induced *in situ,* by cooling hot agarose solutions to 23 °C, yielding a network made of aggregated fibrils of double helices, with a typical mesh size of 100 nm [27] (details in Supplemental Material [28]). Creep experiments start 24 h after gelation to allow for equilibration of the gel; during creep, the time evolution of the strain γ is measured for up to 24 h. Figure 1 shows the strain rate $\dot{\gamma}$ vs t, the time elapsed since the application of a shear stress step σ, for four samples with the same composition and comparable viscoelasticity [32]. In all cases, after an initial elastic jump at $t = 0$, $\dot{\gamma}$ decreases as $\dot{\gamma} \propto t^a$, $a = -0.83 \pm 0.10$. For sample S4, an upturn of $\dot{\gamma}(t)$ occurs at $t \approx 10^4$ s, followed by a fast increase of $\dot{\gamma}$, along with the full relaxation of the normal stress (Fig. S3 [28]),

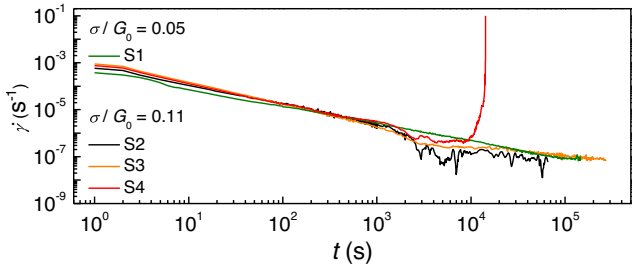

FIG. 1. Shear rate vs time during creep tests, for samples S1–S4. σ is the amplitude of the applied stress and G_0 the gel elastic plateau modulus.

signing the gel macroscopic failure. Remarkably, failure occurs only for S4, although all samples have comparable moduli: For S1–S3, $\dot{\gamma}$ keeps decreasing with the same power law, up to waiting times 10 times longer than the fail time of S4. As expected intuitively, σ must be sufficiently large for macroscopic failure to occur within the duration of the creep measurement ($\geq$24 h). Intriguingly, however, samples can ultimately display drastically different behaviors under a similar load, despite exhibiting the same creep response over several hours.

To rationalize the findings of Fig. 1, we couple light scattering to rheometry. The microscopic dynamics are probed with space and time resolution by acquiring a time series of speckle patterns backscattered by the sample. The images are processed to calculate $c_I(t,\tau,\mathbf{r})$, a local, two-time degree of correlation [33,34] with t the time, τ a time delay, and $\mathbf{r}$ the position in the sample, $\mathbf{r}=0$ being the coordinate of the rheometer axis of rotation [28]. c_I quantifies the amount of microscopic motion over the lag τ, averaged over the sample thickness: $c_I \to 0$ for motion over distances $1/q \gtrsim 30$ nm, with $q = 33.2\ \mu\text{m}^{-1}$ the magnitude of the scattering vector [26].

We show in Fig. 2(a), for a sample of comparable viscoelasticity as those of Fig. 1, a dynamic activity map (DAM) [33] obtained by dividing the imaged area [here, almost the whole sample; see Fig. S2(b) in Ref. [28]] into square regions of interest (ROIs) of side 1.2 mm and plotting for each ROI c_I at a fixed time lag $\tau = 1$ s, with colors ranging from dark red (frozen dynamics, $c_I = 1$) to blue [intense dynamic activity, $c_I < 0.01$, corresponding to a mean square displacement of the scatterers $\Delta r^2(\tau = 1\text{ s}) > 1.4 \times 10^{-2}\ \mu\text{m}^2$]. The DAMs in Fig. 2(a) illustrate the gel dynamics at different times before rupture at $t = t_R = 6210$ s (see also the movie in Ref. [28]). Up to $t_1 = t_R - 2910$ s, approximately at the minimum of the macroscopic shear rate, the dynamics are almost frozen, except for a small region (top of the DAM). Upon approaching failure, this region first expands along the sample rim and then propagates inward (see DAMs at $t_2 = t_R - 82$ s and $t_3 = t_R - 42$ s), until the entire gel exhibits intense dynamics (at $t_4 = t_R - 19$ s). At t_4, the speckle pattern shows radially propagating cracks in the bulk of the gel (see Fig. S6 in Ref. [28]). The inward propagation of intense dynamics is likely due to the heterogeneous strain profile in the plate-plate geometry, for which the local strain is proportional to r. Note, however, that the DAM at the onset of plasticity does not exhibit the same circular symmetry as the strain field. Fast dynamics nucleate in a specific region near the rim, presumably where the gel is weaker, due to heterogeneities in its structure. The nucleation of this dynamically active region about 3000 s before rupture constitutes a remarkable dynamic precursor of failure (see movies and Fig. S7 in Ref. [28] for DAMs from other experiments).

The DAMs in Fig. 2 highlight the rearrangement dynamics on short timescales, $\tau = 1$ s. To explore the timescale dependence of the dynamics, we compute c_I at various τ during the creep tests of samples S1–S4 shown in Fig. 1, enlarging a small area of size 2×1 mm^2 [see Fig. S2(c) in Ref. [28]]. The region is chosen so as to minimize the trivial contribution to c_I arising from the affine deformation of the sample during creep [28]. Data for the four samples are show in Fig. S5 in Ref. [28]. Figure 3(a) focuses on sample S4, during the last 900 s before failure, at $t_R = 11825$ s. The drops of c_I reflect plastic rearrangements leading to enhanced microscopic dynamics. For $\tau = 2$ s, $c_I(t,\tau)$ exhibits an abrupt drop at $t \approx 11500$ s, a few

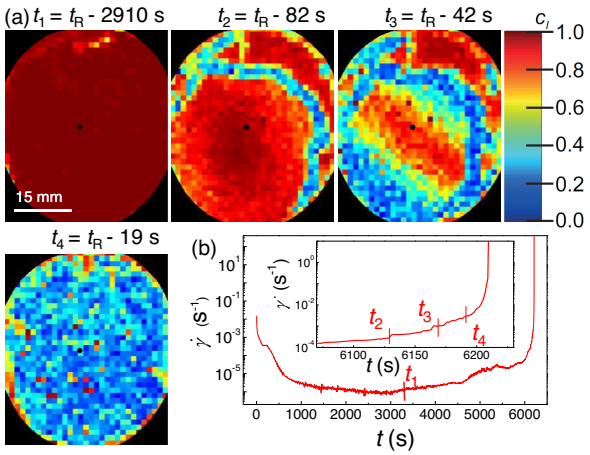

FIG. 2. (a) Dynamic activity maps quantifying the dynamics over a time delay $\tau = 1$ s, measured at four times before rupture, at $t_R = 6210$ s. The black points indicate the plate rotation axis. (b) Creep curve showing t_1 (main plot) and $t_2 - t_4$ (inset).

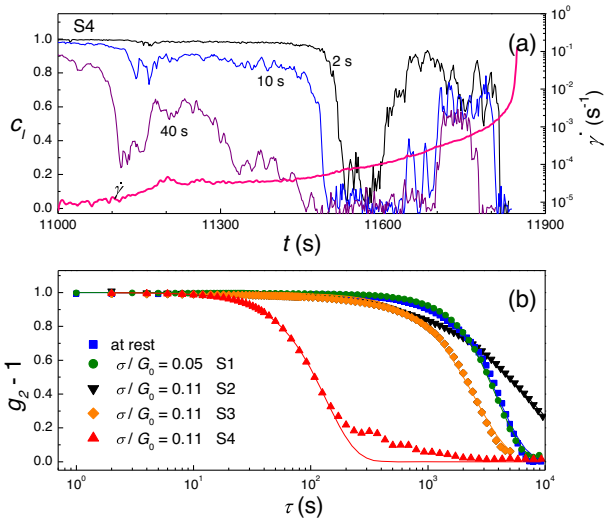

FIG. 3. (a) Time evolution of the degree of correlation at different delays τ for S4, the sample that will fail. Only the last 900 s before rupture are shown. Thick pink line: shear rate $\dot{\gamma}$. (b) Symbols: intensity correlation functions for the same samples as in Fig. 1. Lines: generalized exponential fits (see the text).

hundreds of seconds before the gel rupture. This sudden drop, followed by a slow recovery, is consistent with a wave of plastic activity, highly localized in time, sweeping the sample, as in Fig. 2(a). c_I traces for longer delays, $\tau = 10$ and 40 s, reveal an additional burst of plasticity around $t = 11100$ s, followed by a progressive acceleration of the dynamics, undetectable when probing the dynamics for $\tau = 2$ s. This constitutes a second dynamic precursor of failure, independent of the first one, based on the evolution of the dynamics on longer timescales.

A third dynamic precursor of failure clearly emerges when plotting $g_2(\tau) - 1$, the t-averaged degree of correlation shown in Fig. 3(b) [35]. Correlation functions for all samples can be fitted with a generalized exponential decay, $g_2(\tau) - 1 = \exp[-(\tau/\tau_c)^p]$. For nonrupturing samples [all curves in Fig. 3(b), except S4], the relaxation time τ_c lies in the range (3000–8000) s [28], comparable to that of a gel at rest (blue squares), suggesting that the microscopic dynamics are not significantly perturbed by the imposed stress. By contrast, for S4, the gel that eventually fails, $\tau_c = 140$ s, more than 20 times shorter than for nonrupturing gels.

Figure 3(b) demonstrates that the ultimate fate of a gel is encoded in its average dynamics during the whole creep experiment, not just on approaching failure. Thus, failing gels must differ from nonrupturing ones since their very formation, as inferred from experiments on colloidal gels although only with macroscopic quantities [36,37]. However, any differences must here be subtle: Conventional rheological quantities such as the storage G' and loss G'' viscoelastic moduli do not allow one to identify beforehand those samples that will fail. Indeed, gels with the same composition consistently have a very similar dependence of linear viscoelasticity on time t_q since starting the cooling ramp to induce gelation. This is shown by the symbols in Fig. 4(a), which display the time evolution of G' and G'' for three distinct gels with the same composition as those in Figs. 1 and 3. By contrast, the time dependence of the normal stress σ_N (lines) exhibits significant sample-to-sample differences. The three lines in Fig. 4(a) are representative of three distinct classes of behavior, based on the evolution of σ_N during gelation and on how the gap H is controlled [38]. When H is kept constant [solid and dotted lines in Fig. 4(a)], a negative σ_N signals the emergence of normal forces that pull the plates together. These forces may relax during gelation, leading to gels with a moderate normal stress plateau σ_N^0 at the end of gelation [$\sigma_N^0 \sim -0.8$ to -5 kPa, continuous line in Fig. 4(a)]. If no relaxation occurs during gelation, $\sigma_N^0 < -5$ kPa (dotted line). We also prepare stress-free samples, obtained by letting the rheometer continuously adjust H to keep $\sigma_N \approx 0$ [dashed line in Fig. 4(a)].

To understand the microscopic mechanisms responsible for the distinct evolutions of σ_N, we plot in Figs. 4(b) and 4(c) the relevant macroscopic quantities together with the evolution of c_I at selected delays τ. Under $\sigma_N \approx 0$ conditions

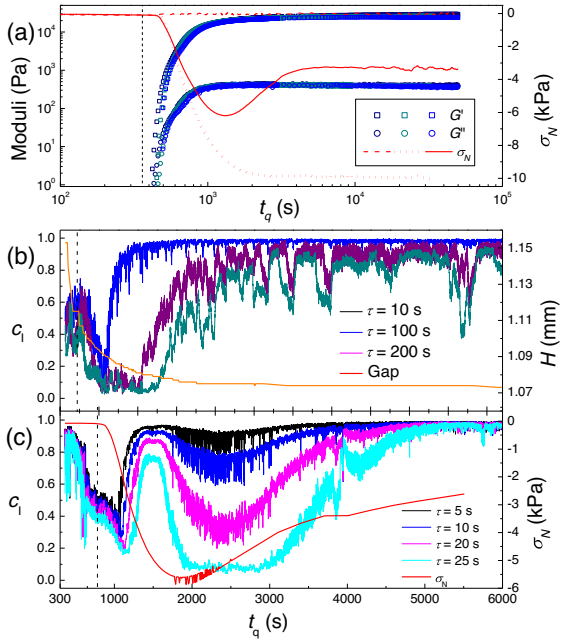

FIG. 4. Evolution with time t_q since quenching the sample at $T = 23\,°C$, of various quantities. (a) Viscoelastic moduli G' and G'' (symbols) and normal stress (lines), for three samples during gelation, at fixed gap H (solid and dotted lines) or adjustable H and $\sigma_N \approx 0$ (dashed line). Vertical line: time at which T reaches 23 °C. (b),(c) Degree of correlation during gelation at variable (b) and fixed (c) gap. In (b), the orange line is the gap evolution. In (c), the red line is $\sigma_N(t)$. The vertical lines in (b) and (c) indicate $G' = G''$.

[Fig. 4(b)], H decreases rapidly at the onset of gelation, due to the emergence of internal tensile forces. This macroscopic reorganization is mirrored by a transient acceleration of the microscopic gel dynamics, signalled by a drop of c_I that lasts until $t_q \sim 900$–1500 s, depending on τ. As gelation proceeds, H tends to stabilize, suggesting less active rearrangements, as confirmed by the c_I traces, which for $t_q \gtrsim 2500$ s reach values close to one, indicative of frozen dynamics. Only sporadic, limited losses of correlation are seen, similar to the "quakes" reported in a variety of gel systems and ascribed to the relaxation of residual internal stresses built up during gelation [39,40].

The scenario is very different when gelation is performed at fixed H [Fig. 4(c)]: A negative σ_N develops as gelation starts; after reaching a minimum (here, ~ -6 kPa), σ_N relaxes, approaching a plateau σ_N^0 (here, ~ -2.5 kPa). The upturn of σ_N is concomitant with a strong, transient acceleration of the microscopic dynamics (nonmonotonic evolution of c_I for 1600 s $\lesssim t_q \lesssim$ 4000 s). Note that the acceleration of the dynamics is much more pronounced here than for the sample with variable H and $\sigma_N \approx 0$, since comparable or even greater drops of c_I are seen over time lags τ significantly smaller than in Fig. 4(b). We conclude that rearrangements during the late stages of gel formation, triggered by the development of strong normal forces, are

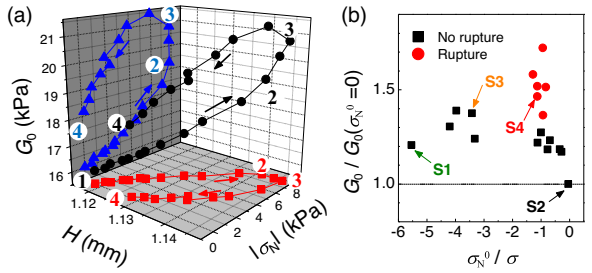

FIG. 5. (a) Black line and symbols: sample trajectory in the $(H, |\sigma_N|, G_0)$ parameter space for an experiment where the gap H is varied. The arrows and numbers indicate the progression along the trajectory. Red (respectively, blue) lines and symbols are the projection of the trajectory on the (H, σ_N) [respectively, (G_0, σ_N)] plane. (b) G_0 normalized by 17.8 kPa, G_0 for sample (S2) with $\sigma_N^0 = 0$, as a function of σ_N^0/σ for gels that eventually did (red circles) or did not (black squares) fail in creep tests. The arrows indicate samples S1–S4 investigated in Figs. 1 and 3.

responsible for the remodeling of the gel and the partial relaxation of σ_N. These rearrangements do not systematically occur in all experiments at fixed H, suggesting random sample-to-sample variations of the gel ability to sustain large normal stresses. Accordingly, for some samples, σ_N decreases monotonically before reaching a plateau [dotted line in Fig. 4(a)].

To rationalize the role of the normal stress on the fate of sheared gels, we design a protocol that reproduces the nonmonotonic behavior of σ_N in a controlled fashion. We induce a change of σ_N through incremental variations of the gap, starting from a relaxed gel ($\sigma_N^0 \approx 0$) and recording at each step both σ_N and the elastic modulus G_0, measured by imposing an oscillatory shear of small amplitude. Figure 5(a) shows the sample trajectory in the parameter space $(H, |\sigma_N|, G_0)$; relevant points along the trajectory are labeled ①–④. Starting from ① and increasing H, $|\sigma_N|$ increases progressively, inducing a smooth growth of G_0, as previously observed for biopolymers [18,38]. As seen by projecting the trajectory on the $(H, |\sigma_N|)$ plane (red line and symbols), beyond point ②, σ_N stops growing with H and reaches a plateau, up to ③. This is the distinctive signature of plastic damage due to the tensile strain imposed to the gel, as confirmed by the observation of hysteresis: Upon reducing H, from ③ to ④, the $\sigma_N = 0$ condition is recovered for a gap H larger than the initial one. The evolution of G_0 is strikingly different from that of σ_N [blue lines and symbols, Fig. 5(a)]. Between ② and ③, the shear modulus *steeply increases* rather than flattening out. This strain hardening is irreversible: When H is reduced to recover $\sigma_N = 0$ in ④, G_0 remains significantly larger than in ①.

Figure 5(a) suggests that, as σ_N becomes too large, bonds sustaining forces along the normal direction are broken, while new bonds are formed in other directions. This anisotropy leads to a gel with a shear modulus significantly higher than in pristine gels but weaker under a tensile stress. We propose that this mechanism is responsible for the failure of our gels under creep. Both the nonmonotonic $\sigma_N(t)$ and the microscopic dynamics shown in Fig. 4 support the occurrence of these plastic rearrangements. As a result, some gels are significantly weakened in their ability to resist normal stresses. Although these gels would have larger G_0, they will paradoxically fail under shear, because biopolymer gels under shear quite generally develop strong tensile stresses [17–21].

We test this hypothesis by analyzing the behavior of a large number of gels with identical composition in creep tests lasting up to one day, focusing on the value of the normal stress plateau σ_N^0 and the shear modulus G_0 at the end of gelation. As shown by the black squares in Fig. 5(b), gels able to sustain large normal stresses ($\sigma_N^0/\sigma < -3$) or which relaxed during gelation ending in a nearly stress-free configuration ($\sigma_N^0/\sigma \gtrsim -1.5$) are able to sustain the extra normal stress developed during creep. Conversely, gels with intermediate σ_N^0, comparable to σ, are susceptible to fail. Among them, all gels that actually failed (red circles) had a nonmonotonic evolution of σ_N and G_0 higher than the typical value of the other gels (G_0 is about 50% higher than for the reference gel, with $\sigma_N^0 = 0$, which does not fail) [41]. This finding demonstrate that the gels that fail underwent rearrangement processes breaking the isotropic distribution of the agarose chains in the gel network. These rearrangements do not significantly change the average structure of the gel, since the average static scattered intensity remains constant. However, they are unambiguously detected from changes in the gel dynamics.

In conclusion, we have unveiled the crucial role of normal stress for the ultimate fate of agarose biopolymer gels under a constant shear load, showing that failure is not related to lack of resistance in the shear direction but rather to weakness under the tensile stress that accompanies shear in these materials. As recently observed for other soft solids [2], macroscopic failure is preceded by several precursors in the microscopic dynamics. These findings pave the way for both anticipating and controlling the nonlinear behavior of biopolymer gels, an important class of soft networks.

We acknowledge financial support from the French Agence Nationale de la Recherche (ANR) (Grant No. ANR-14-CE32-0005, FAPRES) and Centre National d'Etudes Spatiales (CNES). We thank E. Del Gado for fruitful discussions. L. C. acknowledges support from the Institut Universitaire de France.

L. C. and L. R. contributed equally to this work.

*Also at Institut Universitaire de France (IUF), 34095 Paris, France.
†laurence.ramos@umontpellier.fr
‡luca.cipelletti@umontpellier.fr

[1] C. Creton and M. Ciccotti, Fracture and adhesion of soft materials: A review, Rep. Prog. Phys. **79**, 046601 (2016).

[2] L. Cipelletti, K. Martens, and L. Ramos, Microscopic precursors of failure in soft matter, Soft Matter **16**, 82 (2020).

[3] A. J. Kinloch, *Fracture Behaviour of Polymers* (Springer, Netherlands, 2013).

[4] F. Tapia, S. Santucci, and J.-C. Géminard, Fracture reveals clustering in cohesive granular matter, Europhys. Lett. **115**, 64001 (2016).

[5] A. Schmeink, L. Goehring, and A. Hemmerle, Fracture of a model cohesive granular material, Soft Matter **13**, 1040 (2017).

[6] M. I. Smith, R. Besseling, M. E. Cates, and V. Bertola, Dilatancy in the flow and fracture of stretched colloidal suspensions, Nat. Commun. **1**, 114 (2010).

[7] S. Aime, L. Ramos, and L. Cipelletti, Microscopic dynamics and failure precursors of a gel under mechanical load, Proc. Natl. Acad. Sci. U.S. A. **115**, 3587 (2018).

[8] D. Bonn, H. Kellay, M. Prochnow, K. Ben-Djemiaa, and J. Meunier, Delayed fracture of an inhomogeneous soft solid, Science **280**, 265 (1998).

[9] T. Baumberger, C. Caroli, and D. Martina, Solvent control of crack dynamics in a reversible hydrogel, Nat. Mater. **5**, 552 (2006).

[10] T. Baumberger, C. Caroli, and D. Martina, Fracture of a biopolymer gel as a viscoplastic disentanglement process, Eur. Phys. J. E **21**, 81 (2006).

[11] L. M. Barrangou, C. R. Daubert, and E. Allen Foegeding, Textural properties of agarose gels. I. Rheological and fracture properties, Food Hydrocolloids **20**, 184 (2006).

[12] M. J. Buehler and T. Ackbarow, Fracture mechanics of protein materials, Mater. Today **10**, 46 (2007).

[13] K. E. Daniels, S. Mukhopadhyay, Paul J. Houseworth, and R. P. Behringer, Instabilities in droplets spreading on gels, Phys. Rev. Lett. **99**, 124501 (2007).

[14] C. Spandagos, T. B. Goudoulas, P. F. Luckham, and O. K. Matar, Surface tension-induced gel fracture. Part 1. Fracture of agar gels, Langmuir **28**, 7197 (2012).

[15] M. Leocmach, C. Perge, T. Divoux, and S. Manneville, Creep and fracture of a protein gel under stress, Phys. Rev. Lett. **113**, 038303 (2014).

[16] B. Mao, A. Bentaleb, F. Louerat, T. Divoux, and P. Snabre, Heat-induced aging of agar solutions: Impact on the structural and mechanical properties of agar gels, Food Hydrocolloids **64**, 59 (2017).

[17] P. A. Janmey, M. E. McCormick, S. Rammensee, J. L. Leight, P. C. Georges, and F. C. MacKintosh, Negative normal stress in semiflexible biopolymer gels, Nat. Mater. **6**, 48 (2007).

[18] A. J. Licup, S. Münster, A. Sharma, M. Sheinman, L. M. Jawerth, B. Fabry, D. A. Weitz, and F. C. MacKintosh, Stress controls the mechanics of collagen networks, Proc. Nat. Acad. Sci. **112**, 9573 (2015).

[19] H. C. G. de Cagny, B. E. Vos, M. Vahabi, N. A. Kurniawan, M. Doi, G. H. Koenderink, F. C. MacKintosh, and D. Bonn, Porosity Governs Normal Stresses in Polymer Gels, Phys. Rev. Lett. **117**, 217802 (2016).

[20] T. Yamamoto, Y. Masubuchi, and M. Doi, Large network swelling and solvent redistribution are necessary for polymer gels to show negative normal stress, ACS Macro Lett. **6**, 512 (2017).

[21] K. Baumgarten and B. P. Tighe, Normal Stresses, Contraction, and Stiffening In Sheared Elastic Networks, Phys. Rev. Lett. **120**, 148004 (2018).

[22] H. J. Kong, E. Wong, and D. J. Mooney, Independent control of rigidity and toughness of polymeric hydrogels, Macromolecules **36**, 4582 (2003).

[23] E. Heymann, Studies on sol-gel transformations. I. The inverse sol-gel transformation of methylcellulose in water, Trans. Faraday Soc. **31**, 846 (1935).

[24] T. A. J. Payens and T. Snoeren, The effect of simple electrolytes on the sol-gel transition of κ-carrageenan, J. Electroanal. Chem. **37**, 291 (1972).

[25] A. H. Clark and S. B. Ross-Murphy, Structural and mechanical properties of biopolymer gels, Adv. Polym. Sci. **83**, 57 (1987).

[26] A. Pommella, A.-M. Philippe, T. Phou, L. Ramos, and L. Cipelletti, Coupling Space-Resolved Dynamic Light Scattering and Rheometry to Investigate Heterogeneous Flow and Nonaffine Dynamics in Glassy and Jammed Soft Matter, Phys. Rev. Applied **11**, 034073 (2019).

[27] M. Djabourov, K. Nishinari, and S. B. Ross-Murphy, *Physical Gels from Biological and Synthetic Polymers* (Cambridge University Press, Cambridge, England, 2013).

[28] See Supplemental Material at http://link.aps.org/supplemental/10.1103/PhysRevLett.125.268006 for more details on the experiments, on the two-time degree of correlation and on the affine contribution during creep experiments, and for additional mechanical and light scattering data on agarose gels under creep, which includes Refs. [29–31].

[29] M. Christel, R. Yahya, M. Albert, and B. A. Antoine, Stick-slip control of the Carbopol microgels on polymethyl methacrylate transparent smooth walls, Soft Matter **8**, 7365 (2012).

[30] E. Poptoshev and P. M. Claesson, Forces between glass surfaces in aqueous polyethylenimine solutions, Langmuir **18**, 2590 (2002).

[31] J.-P. Bouchaud and E. Pitard, Anomalous dynamical l ight scattering in soft glassy gels, Eur. Phys. J. E **6**, 231 (2001).

[32] The elastic modulus G_0 of the samples is shown in Fig. 5(b) and will be discussed later.

[33] A. Duri, D. A. Sessoms, V. Trappe, and L. Cipelletti, Resolving Long-Range Spatial Correlations in Jammed Colloidal Systems Using Photon Correlation Imaging, Phys. Rev. Lett. **102**, 085702 (2009).

[34] L. Cipelletti, G. Brambilla, S. Maccarrone, and S. Caroff, Simultaneous measurement of the microscopic dynamics and the mesoscopic displacement field in soft systems by speckle imaging, Opt. Express **21**, 22353 (2013).

[35] The time average is performed over the duration of the creep experiment, excluding the first 1000 s, when the dynamics are faster because of the stress step imposed at $t = 0$. For S4, we also exclude the last 1000 s before failure, when the dynamics accelerate as discussed above.

[36] J. Sprakel, S. B. Lindström, T. E. Kodger, and D. A. Weitz, Stress Enhancement in the Delayed Yielding of Colloidal Gels, Phys. Rev. Lett. **106**, 248303 (2011).

[37] A. Helal, T. Divoux, and G. H. McKinley, Simultaneous Rheoelectric Measurements of Strongly Conductive Complex Fluids, Phys. Rev. Applied **6**, 064004 (2016).

[38] B. Mao, T. Divoux, and P. Snabre, Normal force controlled rheology applied to agar gelation, J. Rheol. **60**, 473 (2016).
[39] L. Cipelletti, S. Manley, R. C. Ball, and D. A. Weitz, Universal Aging Features in the Restructuring of Fractal Colloidal Gels, Phys. Rev. Lett. **84**, 2275 (2000).
[40] Z. Filiberti, R. Piazza, and S. Buzzaccaro, Multiscale relaxation in aging colloidal gels: From localized plastic events to system-spanning quakes, Phys. Rev. E **100**, 042607 (2019).
[41] The loss moduli are also higher for the gels that fail than for the other gels; see Fig. S8 in Ref. [28].